Electronic Supplementary Information

Spatially Controlled Synthesis of Superlattice-Like SnS/Nitrogen-Doped Graphene Hybrid Nanobelts as High-Rate and Durable Anode Materials in Sodium-Ion Batteries

Lei Wang,[a+] Xiaofang Li,[a+] Zhenzhen Jin, [b+] Zhun Liang,[c] Xiang Peng,[d] Xiaochuan Ren,[a] Biao Gao, [e] Guang Feng,[c] Paul K. Chu [e] and Kaifu Huo*,[a]

[a.] *Wuhan National Laboratory for Optoelectronics, Huazhong University of Science and Technology, Wuhan 430074, China. E-mail: kfhuo@hust.edu.cn*

[b.] *School of Chemistry and Chemical Engineering, Huazhong University of Science and Technology, Wuhan 430074, China.*

[c.] *School of Energy and Power Engineering, Huazhong University of Science and Technology, Wuhan 430074, China.*

[d.] *Department of Physics and Department of Materials Science and Engineering, City University of Hong Kong, Tat Chee Avenue, Kowloon, Hong Kong, China*

[e.] *The State Key Laboratory of Refractories and Metallurgy, Institute of Advanced Materials and Nanotechnology, Wuhan University of Science and Technology, Wuhan 430081, China.*

List of Contents

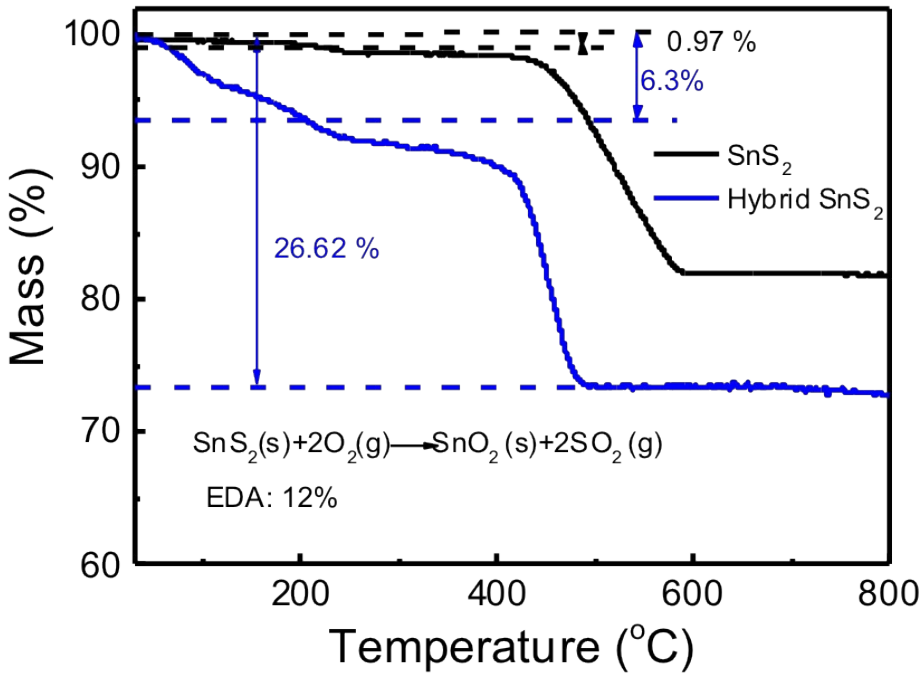

Fig. S1: the TGA for SnS_2 nanobelt and hybrid SnS_2 nanobelt.

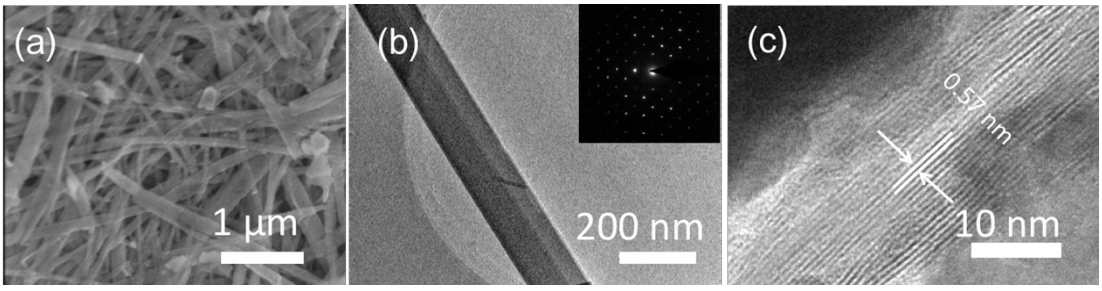

Fig. S2: The morphology characterizations for SnS obtained by annealing the SnS_2 nanobelts under Ar: SEM (a), TEM with SAED inserted (b) and HRTEM (c).

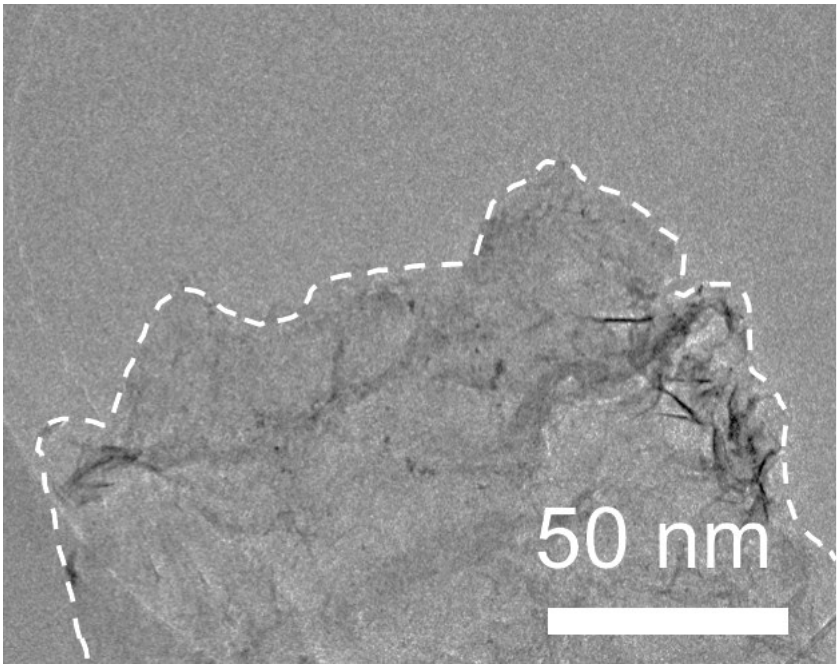

Fig. S3: The TEM image of NG after removal of SnS from SnS/NG hybrid nanobelts

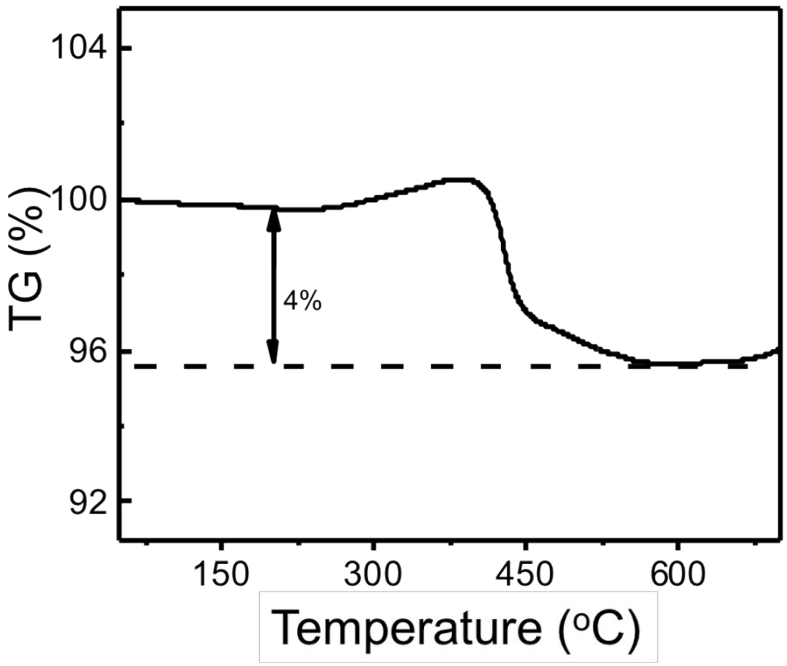

Fig. S4: The TGA profile for SnS/NG hybrid nanobelts

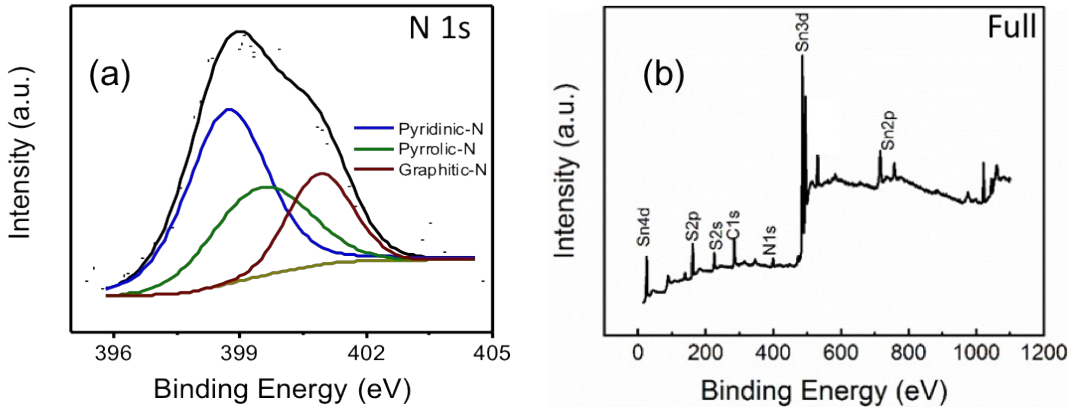

Fig. S5: The XPS spectrum for SnS/NG hybrid nanobelts: (a) the fine spectrum of N1s and (b) the survey spectrum.

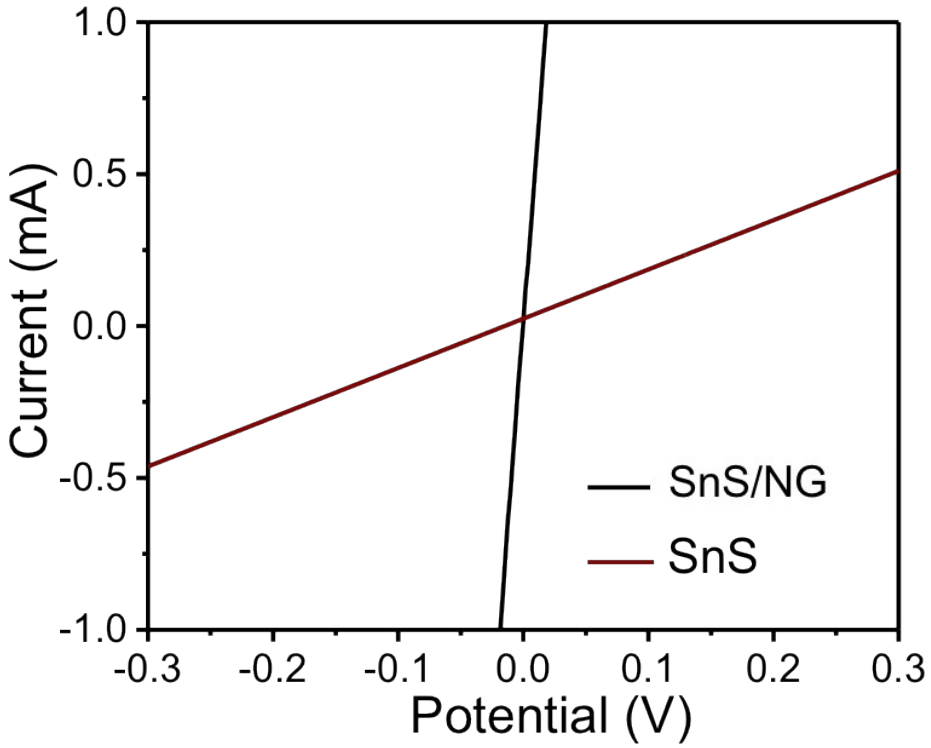

Fig. S6 the I-V profile for SnS and SnS/NG hybrid nanobelts.

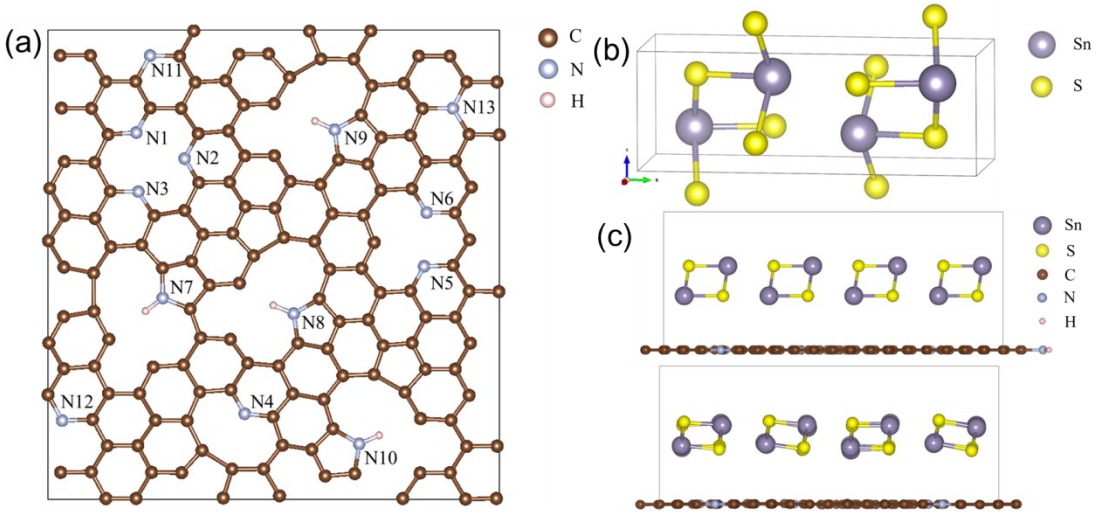

Fig. S7: (a) The optimized structure of NG. N1~N6 are pyridinic-N atoms, N7~N10 are pyrrolic-N atoms and N11~N13 are graphitic-N atoms; (b) The structure of SnS unit cell; (c) The original and optimized structure of SnS/NG heterostructure.

The formation energy of SnS/NG heterostructure system is calculated as Equation 1 to determine the stability of SnS and NG hybrid heterostructure.

$$E_f = (E_{SnS} + E_{NG} - E_{SnS/NG})/n \quad (1)$$

$E_{SnS/NG}$is the total energy of SnS/NG heterostructure; E_{SnS} and $E_{NG}$are the total relaxation energies of SnS supercell and NG, respectively. n is the total number of atoms in the studied systems, which is equal to 249 herein. The formation energy of each atom is about 0.18 eV according to this definition, which indicates that the heterostructure is stable enough[1].

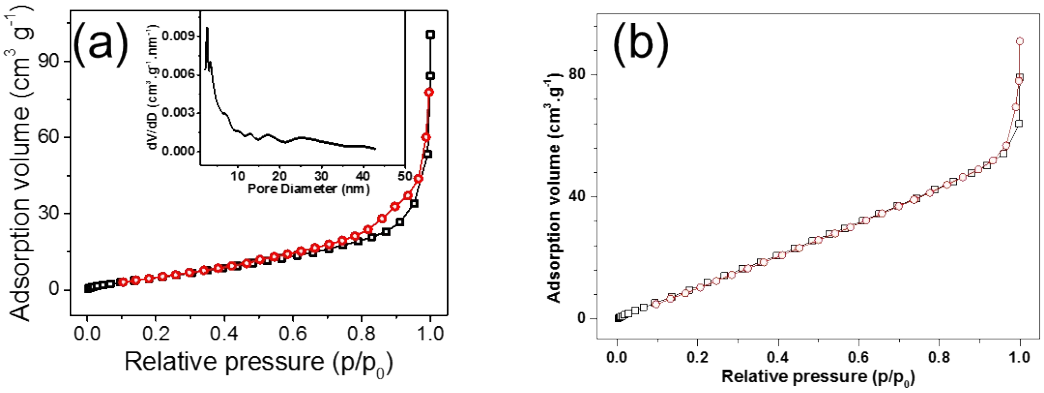

Fig. S8: the isothermal profiles and the corresponding pore size distribution (insert) for SnS/NG (a) and SnS (b)

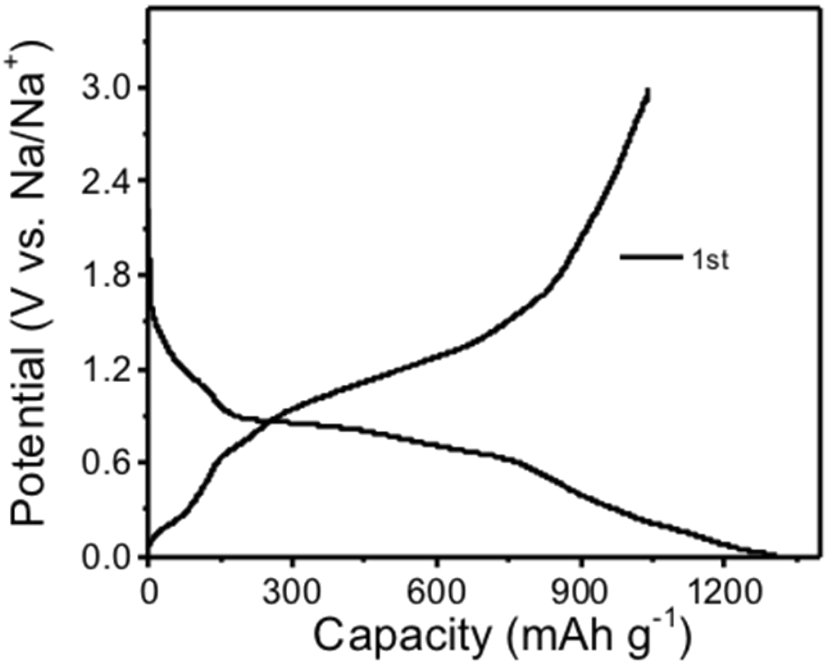

Fig. S9: the galvanostatic charge/ discharge (GCD) profiles for SnS/NG hybrid nanobelts anode during the 1st cycle

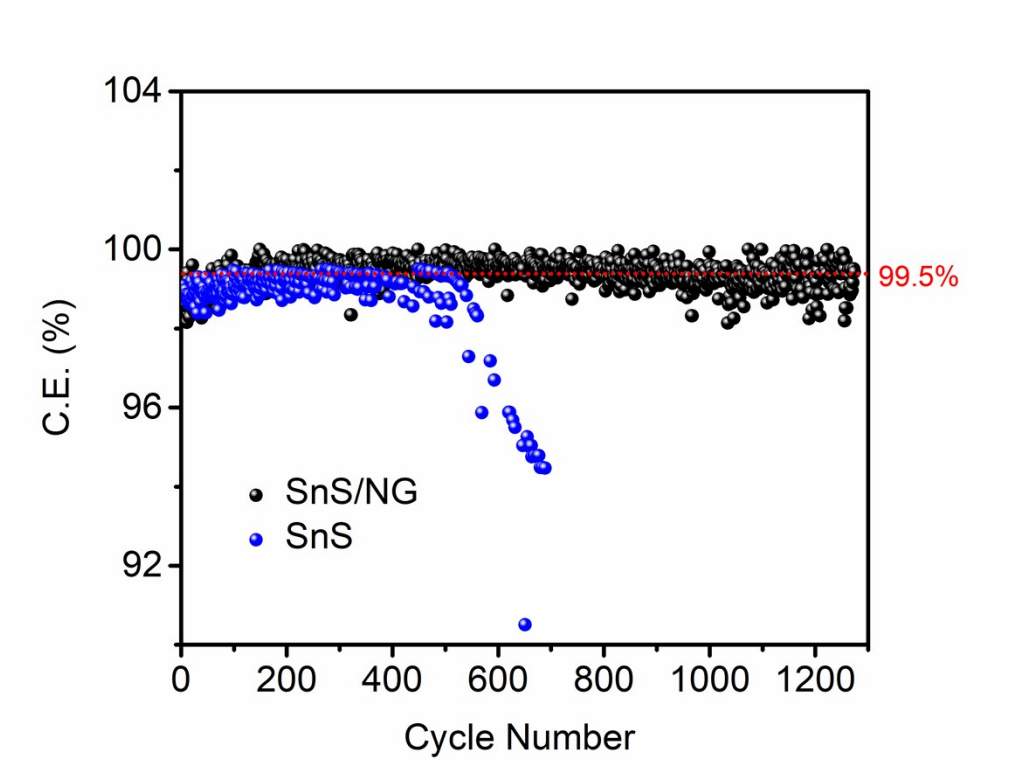

Fig. S10: The coulomb efficiency for the SnS/NG and SnS during cycling tests.

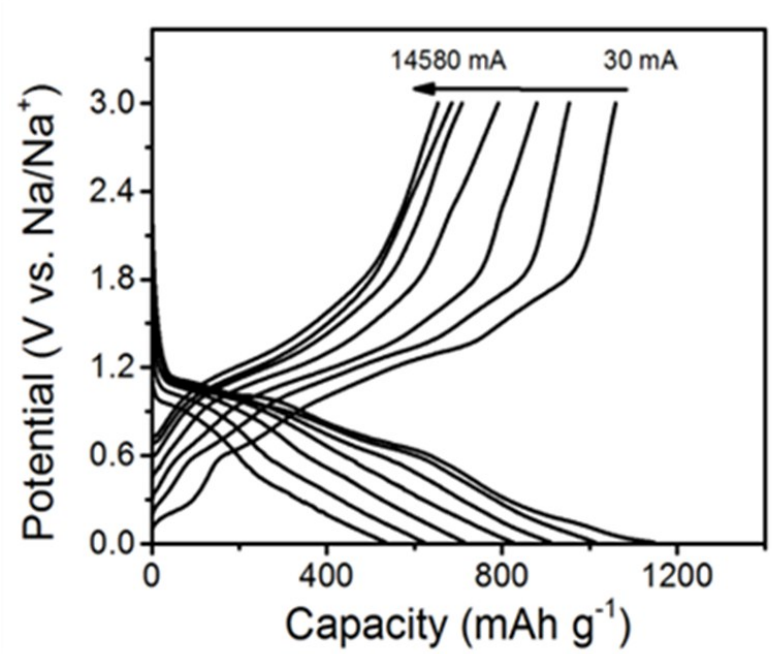

Fig. S11: the GCD profiles for SnS/NG at various current densities.

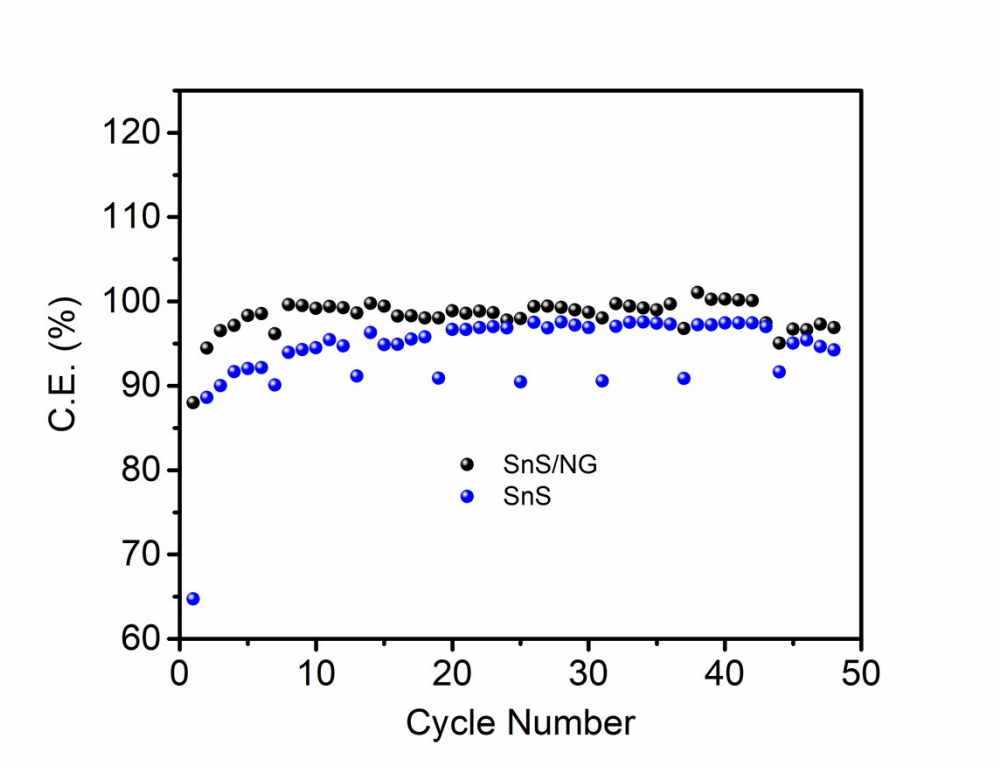

Fig. S12: The coulomb efficiency for the SnS/NG and SnS at different rates.

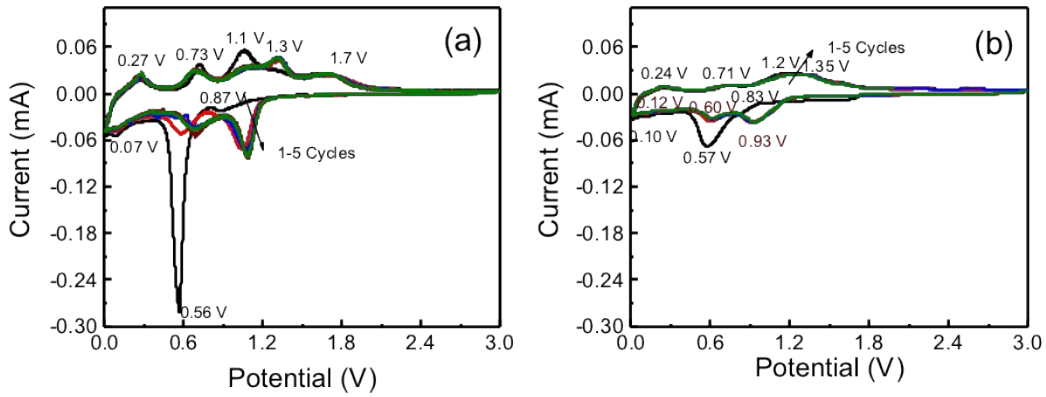

Fig. S13: The cyclic voltage profiles for SnS/NG hybrid (a) and SnS(b).

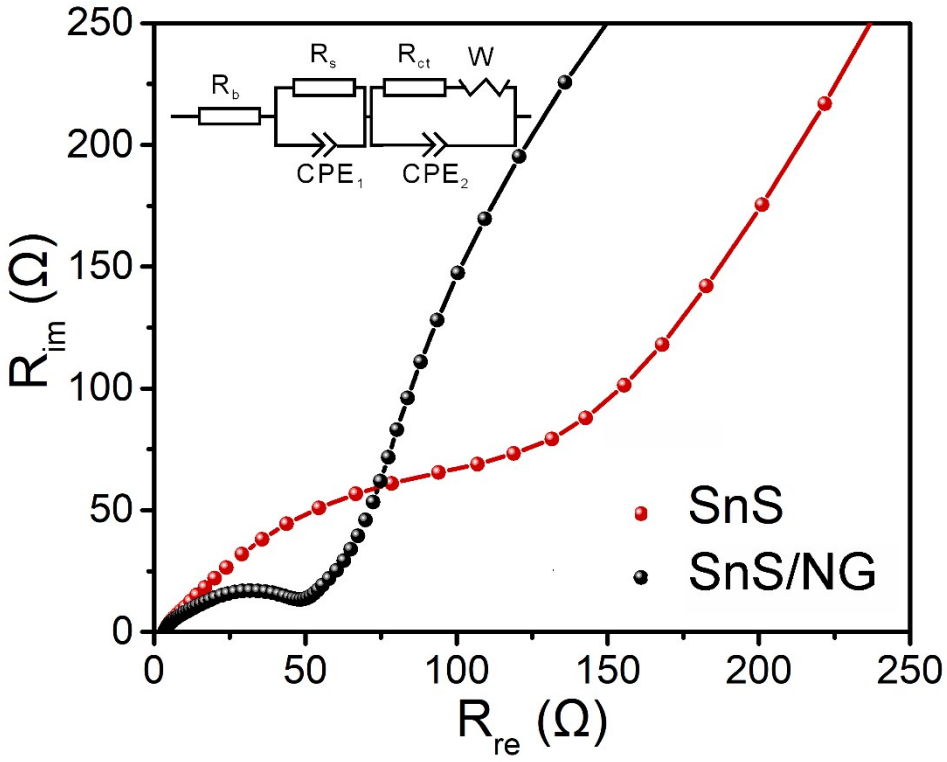

Fig. S14: EIS measurement and the corresponding equivalent circuit and fitting results of SnS and SnS/NG.

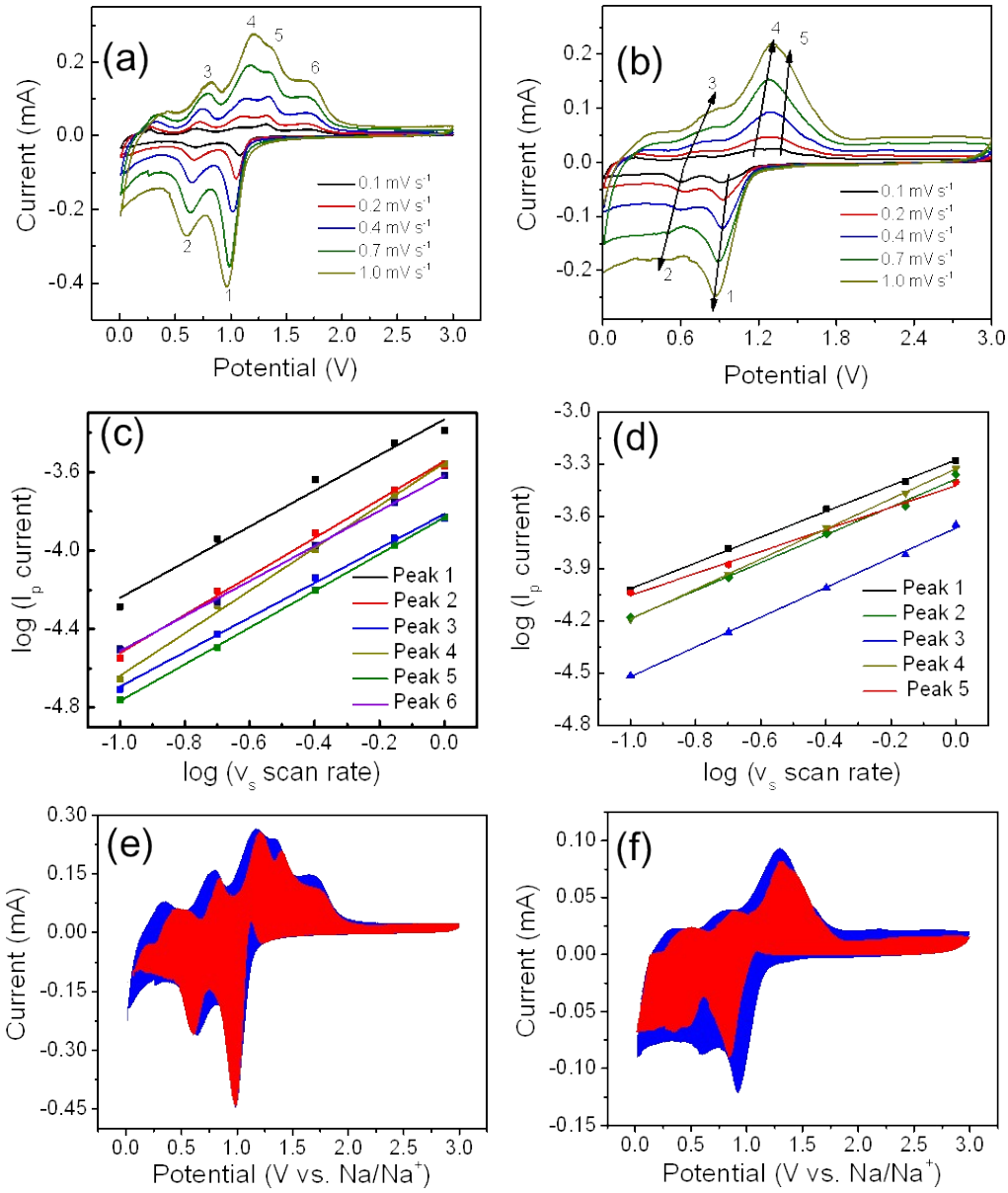

Fig. S15: Cyclic voltammetry profiles for SnS/NG (a) and SnS (b) at different scan rates; the linear fit of peaks intensity and scan rate for SnS/NG (c) and SnS (d), respectively; typical capacitive (red) and diffusion-controlled (blue) contribution to charge storage of SnS/NG (e) and SnS (f). The slops of (c,d) are concluded in the **Table S2**.

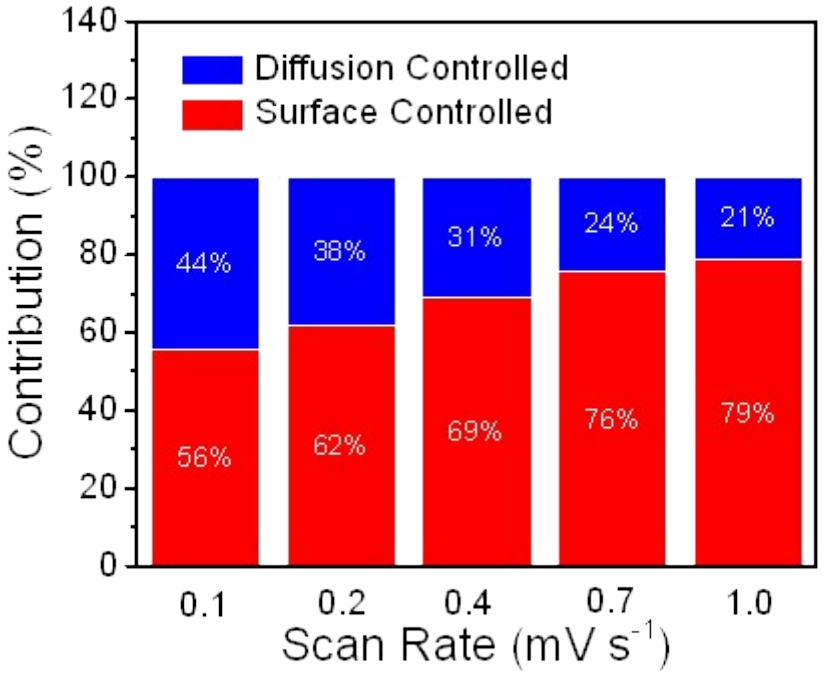

Fig. S16: Normalized contribution ratio of surface controlled (red) and diffusion-controlled (blue) capacities at different scan rate for pure SnS.

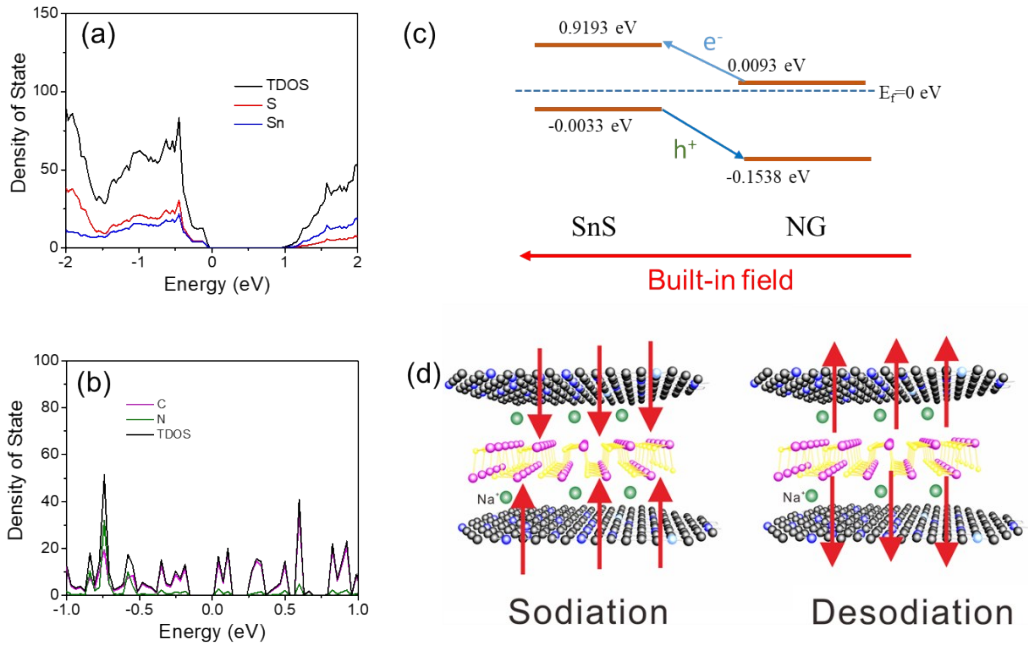

Fig. S17 The DOS profiles for SnS (a) and NG (b); energy band diagrams of interfacial SnS/NG (c); Schematic illustration of the enhanced ion transportation mechanisms of the SnS/NG heteroarchitecture in the SIB system.

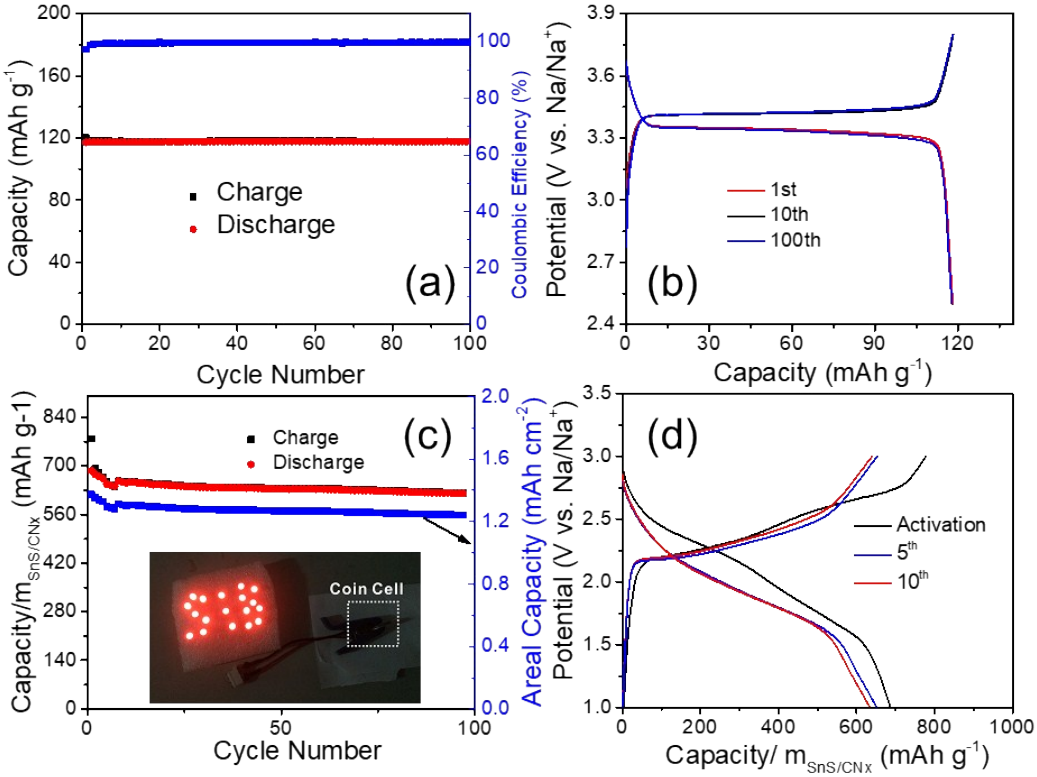

Fig. S18: Full cell demonstration based on $Na_3V_2(PO_4)_3$/C cathode and SnS/NG nanobelts anode: (a) cycle stability and (b) galvanostatic charge/ discharge profiles for $Na_3V_2(PO_4)_3$/C cathode; the cycle ability (c) and galvanostatic charge/ discharge profiles for $Na_3V_2(PO_4)_3$/C // SnS/NG full cell (d). The insert in (c) demonstrates that the full cell can power up 18 red LEDs.

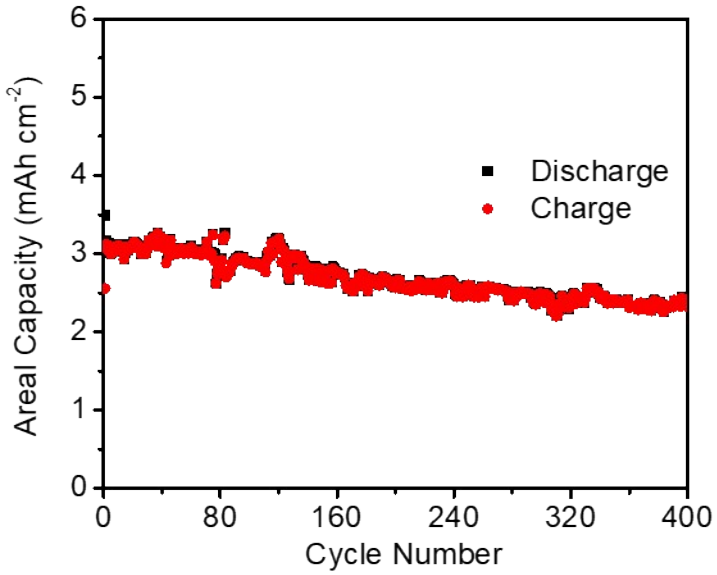

Fig. S19 Cycling performance for full cells with areal capacity of 3 mAh cm^{-2}

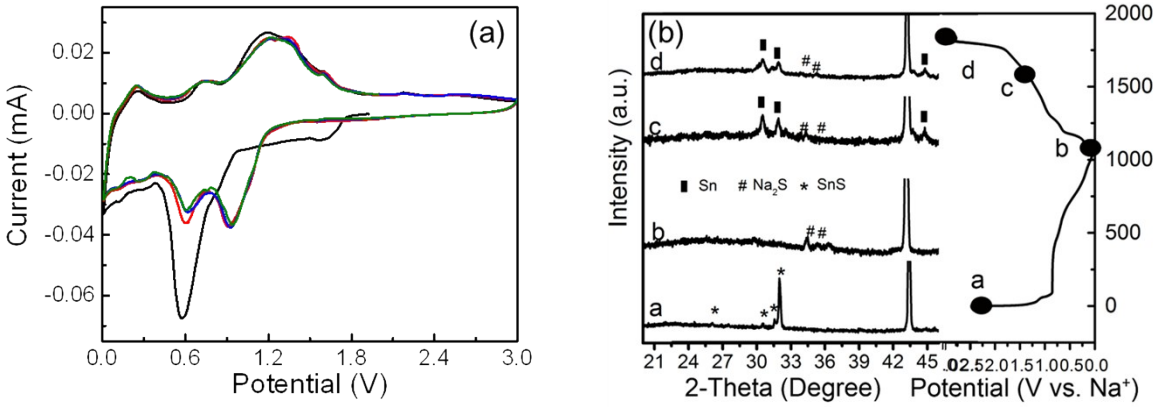

Fig. S20: the cyclic voltammetry profiles(a) and *ex-situ* XRD (b) for SnS.

Table S1: the comparison of electrochemical performance for SnS composite

Sample	C content (wt.%)	Cycling performance (mAh g^{-1}@mA g^{-1}@cycle)	ICE (%)	Rate performance (mAh g^{-1}@mA g^{-1})	Ref.
SnS/G	13.8	492@810@250	65	308@7290	2
GF–SnS NH	~	1010@100@200	80	400@30000	3
SnS@3DGN	8.1	509@2000@1000	80.1	404.8@6000	4
C@SnS/SnO_2@Gr	31	520@500@810	74.6	430@2430	5
3D SnS/C	31	535@300@1000	79	145@10000	6
SnS-C	25	433@500@50	72	280@5000	7
SnS-C	~	548@100@80	66	452@800	8
SnS/CNTs	34.5	364@50@100	-	126@3200	9
SnS/C+G	23.5	598@50@30	78.2	458@500	10
5-SnS/C	43.96	517.6@1000@200	75	428.5@5000	11
SnS@RGO	21.9	386@100@100	60	240@400	12
Sn-SnS-C	~	407@100@150	59.6	348@800	13
SnS@NC	-	443@500@100	76.5	456@1000	14
SnS@C-rGO	45.1	524@100@100	62	336@1600	15
SnS/NG	4	590@1600@1200	88.3	540@14580	Our Work

Table S2: the summarized absolute slop for profiles in Figure S12c and d.

Peak	SnS/NG	SnS
1	0.909	0.739
2	0.978	0.631
3	0.879	0.854
4	1.002	0.864
5	1.084	0.799
6	0.893	_

Appendix 1:

Evaluation of enhancement of Na^+ diffusion coefficient

The Na^+ diffusion coefficient (D_{Na+}) can be calculated according to the equations[16, 17]:

$$D_{Na+} = \frac{R^2T^2}{2A^2n^4F^4C^2\sigma^2} \quad (1)$$

Where R is the gas constant(8.314 J mol^{-1} K^{-1}), T is the absolute temperature, A is the area of electrode, n is the number of electrons per molecule during oxidation, F is the Faraday constant (96500 C mol^{-1}), C is the concentration of sodium ions and σ is the Warburg factor, which is a correlation between the real axis of resistance(R_{re}) and the reciprocal square root of the frequency ($\omega^{-1/2}$) in the low-frequency region:

$$R_{re} = R_e + R_{sei} + R_{ct} + \sigma\omega^{-1/2} \quad (2)$$

For the SnS based materials tested at same conditions, the other parameters in equation (1) are almost the same, and from the equation (1) we can see the Na^+ diffusion coefficient is in proportional with $\frac{1}{\sigma^2}$. Base on the above sets, in our comparation for SnS and SnS/NG, we can evaluate the enhancement (E) of Na^+ diffusion coefficients by:

$$E = \frac{D_{Na+}(SnS/NG)}{D_{Na+}(SnS)} = \frac{\sigma(SnS)^2}{\sigma(SnS/NG)^2} \quad (3)$$

Where $D_{Na+}(SnS/NG)$, $D_{Na+}(SnS)$ is the Na^+ diffusion coefficient for SnS/NG and SnS, respectively. According to the equation (2), $\sigma(SnS/NG)$ and $\sigma(SnS)$ are the slops of plots for linear fitting between the real axis of resistances (R_{re}) and the reciprocal square root of the frequency ($\omega^{-1/2}$) in the low-frequency region for SnS/NG and SnS,

respectively.

References

1. A. Samad, M. Noor-A-Alam and Y.-H. Shin, *J. Mater. Chem. A*, 2016, **4**, 14316-14323.
2. T. Zhou, W. K. Pang, C. Zhang, J. Yang, Z. Chen, H. K. Liu and Z. Guo, *Acs Nano*, 2014, **8**, 8323-8333.
3. D. Chao, C. Zhu, P. Yang, X. Xia, J. Liu, J. Wang, X. Fan, S. V. Savilov, J. Lin and H. J. Fan, *Nat. Commun.*, 2016, **7**, 12122.
4. X. Xiong, C. Yang, G. Wang, Y. Lin, X. Ou, J.-H. Wang, B. Zhao, M. Liu, Z. Lin and K. Huang, *Energy Environ. Sci.*, 2017, **10**, 1757-1763.
5. Y. Zheng, T. F. Zhou, C. F. Zhang, J. F. Mao, H. K. Liu and Z. P. Guo, *Angew. Chem. Int. Ed.* 2016, **55**, 3408-3413.
6. C. B. Zhu, P. Kopold, W. H. Li, P. A. van Aken, J. Maier and Y. Yu, *Adv. Sci.*, 2015, **2**, 201500200.
7. S. H. Choi and Y. C. Kang, *Nano Res.*, 2015, **8**, 1595-1603.
8. L. Wu, H. Lu, L. Xiao, J. Qian, X. Ai, H. Yang and Y. Cao, *J. Mater. Chem. A*, 2014, **2**, 16424-16428.
9. S. Zhang, L. Yue, H. Zhao, Z. Wang and J. Mi, *Mater. Lett.*, 2017, **209**, 212-215.
10. Y. C. Lu, C. Ma, J. Alvarado, N. Dimov, Y. S. Meng and S. Okada, *J. Mater. Chem. A*, 2015, **3**, 16971-16977.
11. J. Wang, Y. Lu, N. Zhang, X. Xiang, J. Liang and J. Chen, *Rsc Adv.*, 2016, **6**, 95805-95811.
12. L. Wu, H. Lu, L. Xiao, X. Ai, H. Yang and Y. Cao, *J. Power Sources*, 2015, **293**, 784-789.
13. L. Wu, X. Hu, J. Qian, F. Pei, F. Wu, R. Mao, X. Ai, H. Yang and Y. Cao, *J. Mater. Chem. A*, 2013, **1**, 7181-7184.
14. S. B. Wang, Y. J. Fang, X. Wang and X. W. Lou, *Angew. Chem. Int. Ed.*, 2019, **58**, 760-763.
15. S. Zhang, G. Wang, Z. Zhang, B. Wang, J. Bai and H. Wang, *Small*, 2019, 1900565.
16. Y. G. Sun, J. Tang, K. Zhang, J. S. Yuan, L. A. Jing, D. M. Zhu, K. Ozawa and L. C. Qin, *Nanoscale*, 2017, **9**, 2585-2595.
17. B. N. Yun, H. L. Du, J. Y. Hwang, H. G. Jung and Y. K. Sun, *J. Mater. Chem. A*, 2017, **5**, 2802-2810.